Published OnlineFirst October 19, 2016; DOI: 10.1158/1535-7163.MCT-16-0449

Large Molecule Therapeutics

Molecular Cancer Therapeutics

Preclinical Efficacy of an Antibody–Drug Conjugate Targeting Mesothelin Correlates with Quantitative ^{89}Zr-ImmunoPET

Anton G.T. Terwisscha van Scheltinga[1,2], Annie Ogasawara[1], Glenn Pacheco[1], Alexander N. Vanderbilt[1], Jeff N. Tinianow[1], Nidhi Gupta[1], Dongwei Li[1], Ron Firestein[1], Jan Marik[1], Suzie J. Scales[1], and Simon-Peter Williams[1]

Abstract

Antibody–drug conjugates (ADC) use monoclonal antibodies (mAb) as vehicles to deliver potent cytotoxic drugs selectively to tumor cells expressing the target. Molecular imaging with zirconium-89 (^{89}Zr)-labeled mAbs recapitulates similar targeting biology and might help predict the efficacy of these ADCs. An anti-mesothelin antibody (AMA, MMOT0530A) was used to make comparisons between its efficacy as an ADC and its tumor uptake as measured by ^{89}Zr immunoPET imaging. Mesothelin-targeted tumor growth inhibition by monomethyl auristatin E (MMAE), ADC AMA-MMAE (DMOT4039A), was measured in mice bearing xenografts of ovarian cancer OVCAR-3×2.1, pancreatic cancers Capan-2, HPAC, AsPC-1, and HPAF-II, or mesothelioma MSTO-211H. *Ex vivo* analysis of mesothelin expression was performed using immunohistochemistry. AMA-MMAE showed the greatest growth inhibition in OVCAR-3×2.1, Capan-2, and HPAC tumors, which showed target-specific tumor uptake of ^{89}Zr-AMA. The less responsive xenografts (AsPC-1, HPAF-II, and MSTO-211H) did not show ^{89}Zr-AMA uptake despite confirmed mesothelin expression. ImmunoPET can demonstrate the necessary delivery, binding, and internalization of an ADC antibody *in vivo* and this correlates with the efficacy of mesothelin-targeted ADC in tumors vulnerable to the cytotoxic drug delivered. *Mol Cancer Ther; 16(1); 134–42. ©2016 AACR.*

Introduction

Mesothelin is a tumor antigen highly expressed in ovarian cancer, mesothelioma, and in most pancreatic adenocarcinomas (1, 2). Until now chemotherapy and targeted agents have yielded only modest effects in these tumors. An alternative is to use an antibody–drug conjugate (ADC), consisting of a specific monoclonal antibody (mAb) armed with a cytotoxic drug that will be released after internalization (3). Two recently approved ADCs exemplify monomethyl auristatin E (MMAE) and maytansinoid drug conjugates: brentuximab vedotin for CD30-positive lymphomas and trastuzumab-emtansine (T-DM1) for metastatic breast cancer, respectively (4–6). Mesothelin might also serve as a target for ADCs. In studies with SS1P, a recombinant immunotoxin consisting of an anti-mesothelin variable fragment linked to PE38, a portion of Pseudomonas exotoxin A, several patients showed minor responses (7, 8). Furthermore, various preliminary studies with anti-mesothelin ADCs showed promise, including one anti-mesothelin antibody (AMA) conjugated to the maytansinoid DM4 that exhibited a confirmed partial response in a mesothelioma patient (9); and the AMA–MMAE conjugate DMOT4039A (3, 10), which has produced several confirmed partial responses in ovarian and pancreatic cancers (11).

ADC target antigens are typically chosen because they exhibit tumor-specific expression patterns and, if internalized, represent an entry portal for cytotoxic drugs into cancer cells (12). These antigens are not necessarily molecular drivers of cancer and so can be lost during tumor progression or metastasis, which would impair ADC efficacy, highlighting the need to comprehensively assess and reassess the tumor target status.

The precise dosing of drugs and selection of patients for mesothelin-directed therapy could therefore benefit from noninvasive visualization of AMA distribution to quantify antibody uptake in tumor lesions. The long-lived positron-emitting isotope zirconium-89 (^{89}Zr, half-life: 3.27 days) has been used to radiolabel AMA and enable its noninvasive imaging using immunoPET (13–15). ^{89}Zr-labeled AMA (MMOT0503A) was previously characterized in preclinical models of human pancreatic cancer, which demonstrated the imaging signal was target-specific and dose-dependent (13, 14). Mesothelin imaging has also been performed with a variety of anti-meosthelin antibodies in preclinical models. Specific uptake was measured with ^{111}In-labeled anti-ERC/mesothelin mouse monoclonal and Fab fragment (16) and with ^{64}Cu-labeled 11-25, a murine monoclonal (17). In the clinic, ^{111}Indium (^{111}In)-labeled amatuximab, a chimeric monoclonal, localized to mesothelioma and pancreatic tumors and was well tolerated with a favorable dosimetry profile (18). To confirm

[1]Genentech Research and Early Development, Genentech, Inc,. South San Francisco, California. [2]Department of Clinical Pharmacy and Pharmacology, University Medical Center Groningen, University of Groningen, Groningen, the Netherlands.

Note: Supplementary data for this article are available at Molecular Cancer Therapeutics Online (http://mct.aacrjournals.org/).

Corresponding Author: Simon-Peter Williams, 1 DNA Way, South San Francisco, CA 94080. Phone: 1-650-2254292; Fax: 1-650-7424905; E-mail: williams.simon@gene.com

doi: 10.1158/1535-7163.MCT-16-0449

Published OnlineFirst October 19, 2016; DOI: 10.1158/1535-7163.MCT-16-0449

tumor antibody uptake and predict ADC efficacy, it is preferable to use the same antibody for molecular imaging as in the ADC because different antibodies can have different binding characteristics and internalization rates [indeed, this is the case for mesothelin antibodies to 5 different epitopes (ref. 3 and SJS, unpublished observations)].

This study directly compares tumor growth inhibition following administration of the ADC targeting mesothelin (AMA-MMAE; DMOT4039A; ref. 3) with image-derived measurements of tumor antibody uptake using the ^{89}Zr-labeled AMA in a panel of 6 tumor models. We test the hypothesis that molecular imaging could help predict treatment effects of the AMA-MMAE therapeutic ADC.

Materials and Methods

Characterization of human tumor cell lines

Ovarian OVCAR-3×2.1 (derived at Genentech from NIH-OVCAR3; ref. 3), pancreatic Capan-2 (2008), HPAC (2010), AsPC-1 (2008), and HPAF-II (2009) and mesothelioma MSTO-211H (2010) cells were obtained from ATCC, banked at Genentech, and accessed in the years indicated. Their identity was confirmed by DNA testing (STR profiling) and they lacked mycoplasma contamination. To determine mesothelin surface expression, cells were incubated with 1 μg/mL AMA in FACS buffer (3% FBS in PBS) on ice for 1 hour followed by Alexa488 anti-human antibody (Invitrogen 11013) and analyzed using a FACS Calibur Flow Cytometer (Becton Dickinson) and FlowJo (v8.4.5) software. Scatchard analysis determined surface mesothelin copy numbers with ^{125}I-AMA as previously described (3). Immunofluorescence internalization was performed as described with AMA (3) in the presence of 5 μmol/L pepstatin A and 10 μg/mL leupeptin (Roche), with AMA being detected by Cy3-anti-human and mouse anti-LAMP1 (BD555798) with FITC-anti-mouse following paraformaldehyde fixation and saponin permeabilization. Two-micrometer *z*-stacks of images taken with a 60 × objective were processed by deconvolution microscopy on a DeltaVision microscope and flattened projections are shown.

Antibody–drug conjugates

For tumor growth inhibition studies, AMA-MMAE (DMOT4039A) was prepared from a fully humanized IgG1 AMA (h7D9.v3, MMOT0530A) by conjugation with the auristatin moiety MC-vc-PAB-MMAE as previously described (3, 5). An antibody to HSV-1 viral coat protein gD (humanized IgG1 5B6) was used as a nonbinding isotype control (anti-gD) and was similarly conjugated with MMAE (anti-gD-MMAE). Mouse pharmacokinetic studies have shown that AMA-MMAE has relatively well-behaved dose–linear pharmacokinetic properties in the 1 to 10 mg/kg range (Supplementary Fig. S1A) and that ADC clearance is within 2-fold of the naked antibody (Supplementary Fig. S1B), consistent with other ADCs (19).

Zirconium-89 labeling of antibodies targeting mesothelin and gD

For immunoPET imaging, naked antibodies (without MMAE) were conjugated with desferrioxamine B (DFO) through side-chain lysines using a bifunctional ligand p-SCN-Bn-deferoxamine (DFO; Macrocyclics) chelating group using the benzyl isothiocyanate reagent and radiolabeled with ^{89}Zr (20). Conjugated antibody was stored in 10 mmol/L succinate, 240 mmol/L sucrose, 0.02% polysorbate 20, pH 5.5. After radiolabeling, the ^{89}Zr labeled antibody was formulated in 0.25 mol/L sodium acetate with 5 mg/mL gentisic acid (10%–30% v/v) by buffer exchange using NAP-10 columns (GE Healthcare). Quality control of the conjugated and radiolabeled antibodies was performed as described earlier (14, 20). Endotoxins were determined in a PTS Endosafe (Charles River) assay.

Animal studies

All animal studies were approved by and conducted in accordance to the guidelines of the Institutional Animal Care and Use Committee at Genentech, which is accredited by the American Association for the Advancement of Laboratory Animal Care (AAALAC). Female mice were acclimated at least 1 week prior to study start and were 4 to 5 months old. For all experiments, mice were age-matched and tumors were the same size (250–400 mm^3) for tumor growth inhibition studies and imaging studies.

Cells were prepared for inoculation in HBSS (Gibco) or HBSS and 50% v/v Matrigel (BD Biosciences) and 200 μL was injected into the right dorsal flank. The number of cells inoculated to establish similar-sized tumors were OVCAR-3×2.1, HPAF-II, and MSTO-211H: 10 million cells; Capan-2, HPAC, and AsPC-1: 5 million cells. All were in immunocompromised CB17.SCID.bg mice (Charles River) except HPAF-II (CB17.SCID) and HPAC (Taconic NCR).

Tumor growth inhibition studies

Tumor growth inhibition studies were conducted using a single (suboptimal) dose of 5 mg/kg of AMA-MMAE, an ADC targeting mesothelin, or nontargeting anti-gD-MMAE (isotype control) in tumor-bearing mice. This dose was chosen from prior experience to achieve measurable growth inhibition across a range of models without causing near-complete regressions that would confound interpretation. The same dose was then used for immunoPET imaging studies. A complete tumor growth inhibition study with varying dose levels has been performed before (3). ADCs were administered intravenously via the tail vein (n = 5–8/group). Further studies at 3 and 10 mg/kg were performed in AsPC-1 and Capan-2 with 9 mice per group and in OVCAR3-×2.1 cells with 5 and 20 mg/kg doses (Supplementary Table S1). Tumor length (l, the longest dimension) and width (w, perpendicular to the length) were measured by calipers; tumor volume V was approximated as $V = lw^2/2$.

ImmunoPET imaging studies

For immunoPET experiments, ^{89}Zr-labeled antibodies targeting mesothelin or gD (3.7 MBq, 5 mg/kg in 100 μL) were injected into mice (n = 4–5 per group) via the tail vein. PET imaging was conducted immediately after tracer injection and again 1, 2, 3, and 6 days later using Siemens Inveon PET/CT scanners (Siemens). Animals were lightly anesthetized for restraint with approximately 3.5% sevoflurane, and body temperature was maintained at 37°C by warm airflow. PET scans were 15- to 30-minute static scans.

Region of interest (ROI) measurements were made on multiple axial slices of the tissues using IRW image analysis software (Siemens). An ellipse was drawn tightly around the tumor, and voxels of at least 20% of the maximum intensity were

Published OnlineFirst October 19, 2016; DOI: 10.1158/1535-7163.MCT-16-0449

included in the ROI. Mediastinal blood pool measurements were taken with an elliptical volume in the center of the heart. Decay-corrected signal intensities of tumor and blood were measured as percentages of the injected dose per gram of tissue (%ID/g). Also tumor-to-blood ratios were calculated as another metric of tissue uptake.

Ex vivo tumor analysis

Immunohistochemical (IHC) determination of mesothelin expression was performed on 4-μm sections from formalin-fixed, paraffin-embedded tissues using rabbit anti-mesothelin antibody (SP74, Spring Bioscience; M3744) on a Discovery XT autostainer (Ventana) as before (3). IHC was scored by a certified pathologist (R. Firestein) and is based on the intensity of positive staining observed in at least 50% of tumor cells: "negative" indicates no detectable signal, "1+" is weak, "2+" is moderate, and "3+" is strong.

Immunoprecipitation of xenografts was performed on tumors lysed with Tissue Lyser versus cells lysed in 1% NP40-containing buffer using 5 μg/mL AMA (humanized 7D9.v3) and Western blotted with mouse anti-mesothelin monoclonals 2E5 or 19C3 (Genentech; ref. 3)). Western blotting of cell lines was as described (3) using 2 μg/mL 19C3 antibody and 1:10,000 1A2 anti-tubulin (Sigma T9028) loading control.

Dose dependence of AMA pharmacokinetics in tumor-bearing mice and shed mesothelin levels

Blood concentrations of AMA were determined by ELISA in plasma taken from Capan-2 and AsPC-1 and tumor-bearing mice at 1, 7, and 14 days after dosing at 3 and 10 mg/kg. Shed mesothelin levels were determined using a sensitive ELISA (11).

Statistical analysis

Data are presented as mean ± SD. Statistical analysis was performed using the Mann–Whitney test with GraphPad Prism software. All tests were 2-sided and the significance level was set at $P \leq 0.05$.

Results

Flow cytometric analysis

Cell surface expression of mesothelin was demonstrated by flow cytometry and Scatchard in a panel of 6 cell lines (Fig. 1). The ovarian line OVCAR-3×2.1 showed the highest level of expression, followed by pancreatic Capan-2, HPAC, AsPC-1, and HPAF-II with similar FACS shifts. Mesothelioma MSTO-211H had the lowest surface mesothelin level, in agreement with previous results (3). In all cases, mesothelin expression declined with passaging *in vitro* over time (Fig. 1 and data not shown), as previously reported (3). Similar results were obtained by Western blotting (Fig. 1B).

Tumor growth inhibition studies

Mesothelin-dependent tumor growth inhibition studies (single 5 mg/kg dose, the same as used for immunoPET) of AMA-MMAE (targeted) or gD-MMAE (nontargeted control) showed varying results in the different cell lines (Fig. 2). In OVCAR-3×2.1-bearing mice (Fig. 2A), tumor growth inhibition was significantly greater following treatment with AMA-MMAE than with the control gD-MMAE. Some differential antitumor efficacy was also seen in Capan-2 (Fig. 2B) and

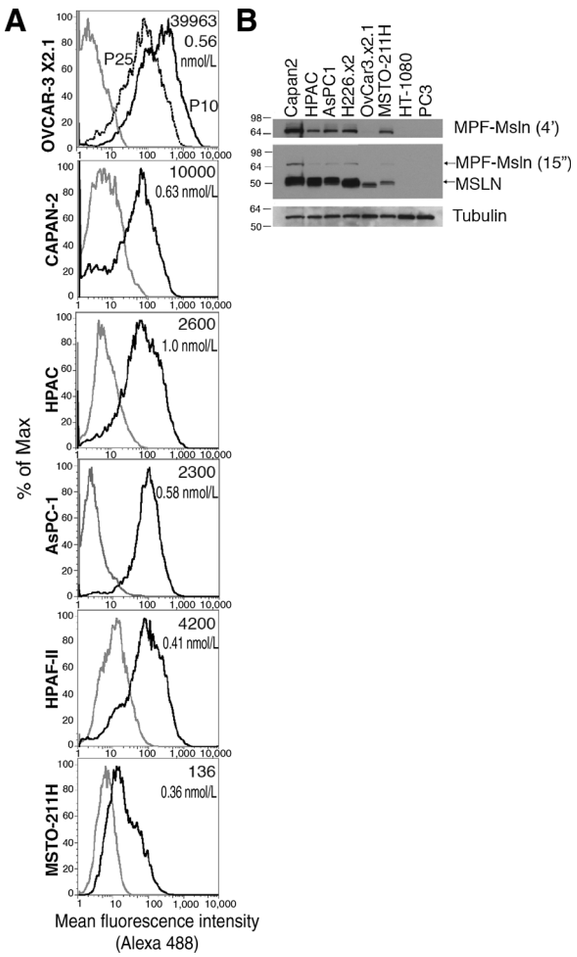

Figure 1.

A, Representative flow cytometric results of mesothelin (black line) expression versus secondary antibody alone (gray line) on all 6 cell lines, with Scatchard-determined copy number and K_ds on the top right. Note mesothelin expression declines with passage (P) number, as exemplified by OVCAR-3×2.1, but is upregulated *in vivo* (see later). **B,** Western blot analysis with mouse anti-mesothelin 19C3 showing surface (mature furin cleaved 50 kDa) versus internal (uncleaved) MPF-mesothelin (71 kDa) levels using P45 OVCAR-3×2.1 and PC3 and HT-1080 cells as mesothelin-negative controls. The top panel was exposed to film for 4 minutes and the middle panel for 15 seconds.

HPAC (Fig. 2C) xenografts. However, AsPC-1 (Fig. 2D), HPAF-II (Fig. 2E), and MSTO-211H (Fig. 2F) tumors showed marginal or no differential efficacy of AMA-MMAE at this dose.

ImmunoPET reagents

^{89}Zr radiolabeled antibodies targeting mesothelin and gD were prepared at ≥80% radiochemical yield and ≥95% radiochemical purity from antibodies averaging 1.6 chelators per antibody. The specific activity of the tracer was more than 63 MBq/mg and was diluted with cold antibody to achieve the desired dose. ^{89}Zr-AMA showed essentially unaltered binding from AMA, IC_{50} values by ELISA being within 10% of the unlabeled antibody (data not shown). Serum stability assays showed less than 10% ^{89}Zr release over 7 days at 37°C, similar

Published OnlineFirst October 19, 2016; DOI: 10.1158/1535-7163.MCT-16-0449

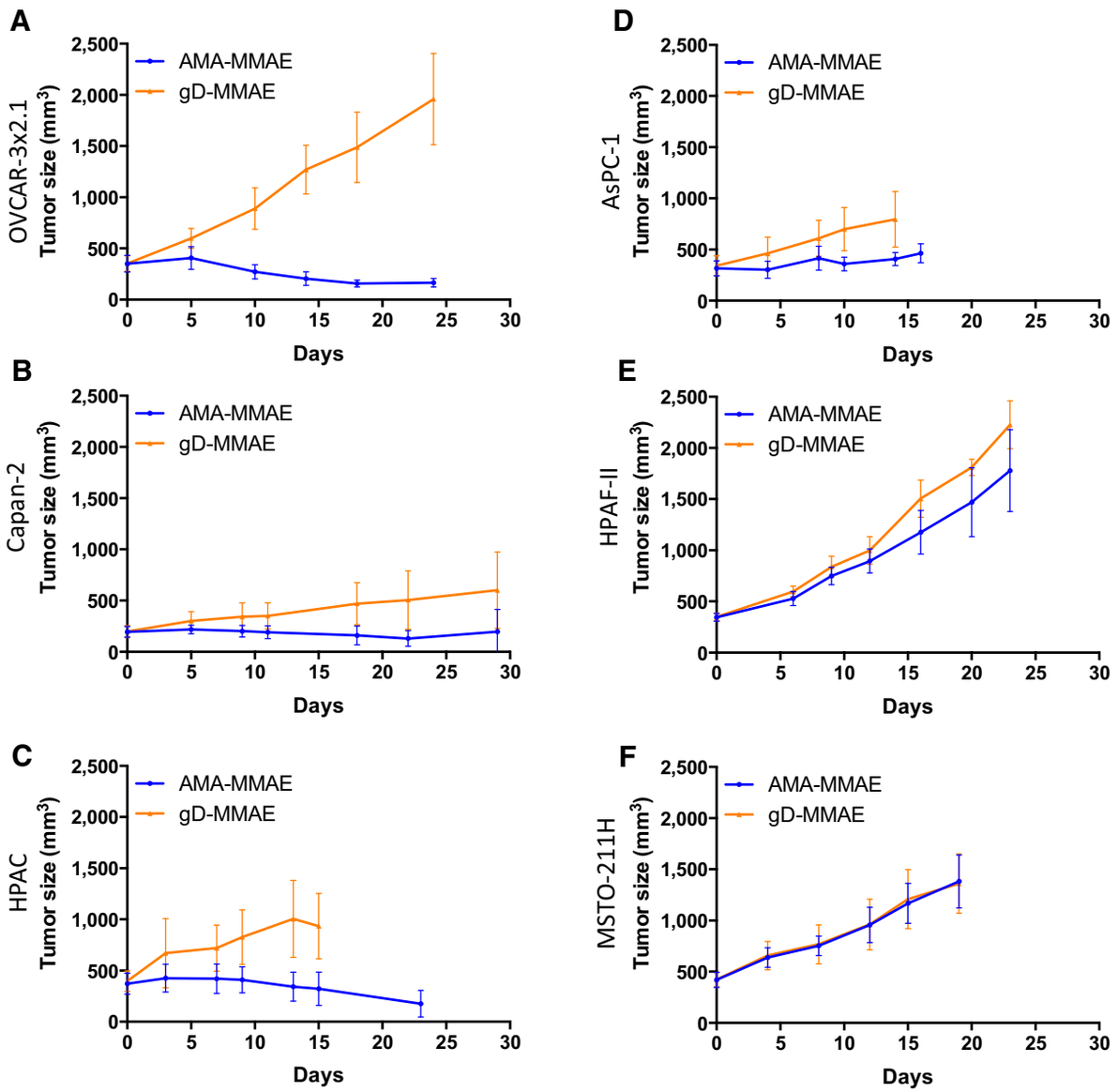

Figure 2.

Tumor growth inhibition studies in xenografted mice after a single suboptimal dose of 5 mg/kg AMA-MMAE (blue) or the nonspecific control gD-MMAE (orange). Tumor volumes were measured up to 4 weeks after dosing for ovarian cancer OVCAR-3×2.1 (**A**); pancreatic cancers Capan-2 (**B**), HPAC (**C**), AsPC-1 (**D**), and HPAF-II (**E**); and mesothelioma MSTO-211H (**F**). Means and SEs are plotted of 5 to 8 mice per group.

to previous reports (13, 14). The endotoxin level was 0.3 EU/mL, suitable for use *in vivo*.

ImmunoPET imaging

For all tumors, ^{89}Zr-AMA and ^{89}Zr-gD uptake is shown between days 0 and 6 after tracer injection (Fig. 3), with maximal uptake reached by day 6. The greatest difference between ^{89}Zr-AMA and nonspecific ^{89}Zr-gD tumor uptake was found in OVCAR-3×2.1 xenografts: 10.4 ± 0.8 %ID/g for ^{89}Zr-AMA versus 4.9 ± 0.7 %ID/g ^{89}Zr-gD at day 6 ($P \leq 0.05$; Fig. 3A). In the other 2 efficacious tumor models, Capan-2 (Fig. 3B) and HPAC (Fig. 3C), ^{89}Zr-AMA tumor uptake was 8.8 ± 1.0 %ID/g and 6.0 ± 1.2 %ID/g, respectively. In all 3 efficacious models, ^{89}Zr-AMA tumor uptake was significantly ($P < 0.05$) higher than ^{89}Zr-gD. In the nonefficacious AsPC-1 (Fig. 3D), HPAF-II (Fig. 3E), and MSTO-211H (Fig. 3F) xenografts, measureable tumor uptake was observed with ^{89}Zr-AMA but was similar to nonspecific ^{89}Zr-gD uptake.

To further compare tumor uptake of ^{89}Zr-AMA and ^{89}Zr-gD, tumor-to-blood ratios were calculated between days 0 and 6 after tracer injection (Fig. 3). These results confirmed those above, showing significantly higher ($P < 0.05$) tumor-to-blood ratios for ^{89}Zr-AMA versus ^{89}Zr-gD in the ADC-responsive OVCAR-3×2.1, Capan-2, and HPAC tumors between 1 and 6 days, but not in the 3 nonresponders.

Published OnlineFirst October 19, 2016; DOI: 10.1158/1535-7163.MCT-16-0449

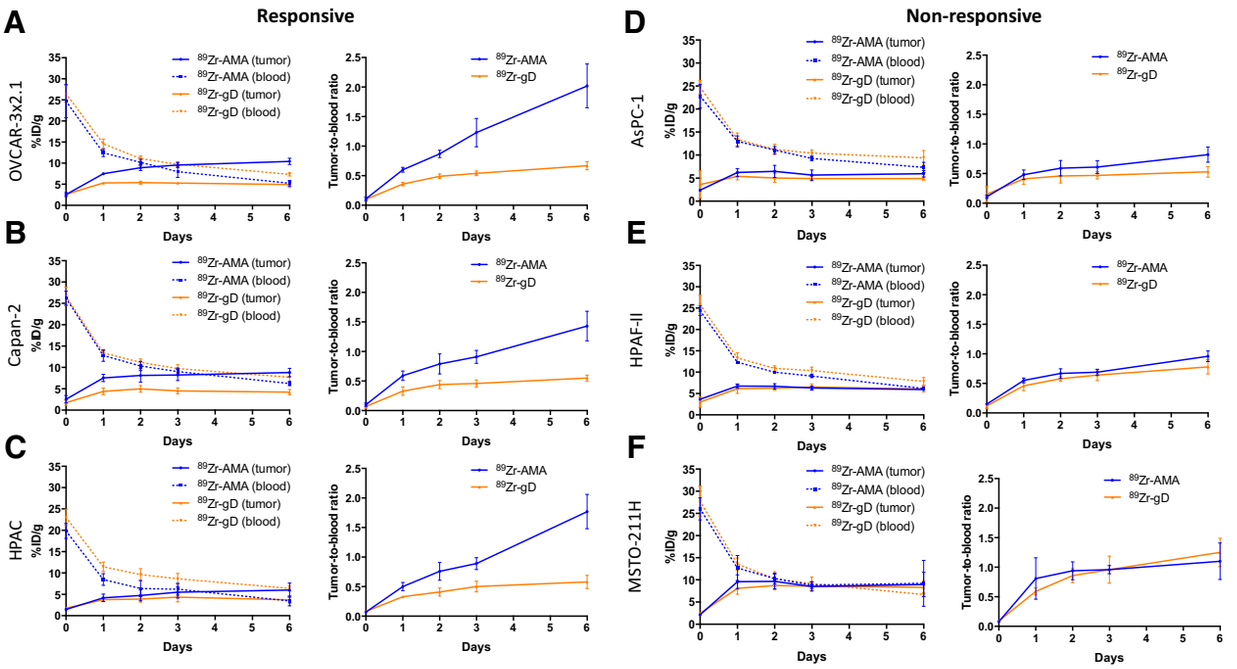

Figure 3.

PET quantification results of tumor uptake (solid lines), blood values (dashed lines), and tumor-to-blood ratios of ^{89}Zr-AMA (blue) and ^{89}Zr-gD (orange). Tracer uptake was measured after a single dose of 5 mg/kg ^{89}Zr-AMA or ^{89}Zr-gD. PET quantification was performed in mice bearing ovarian cancer OVCAR-3×2.1 (**A**); pancreatic cancers Capan-2 (**B**), HPAC (**C**), AsPC-1 (**D**), and HPAF-II (**E**); and mesothelioma MSTO-211H (**F**; mean and SEM of 4 to 5 per group). Tumor and blood values of the tracer are expressed as percentage of the injected dose per gram (%ID/g).

In Fig. 4, representative maximum intensity projections from mouse coronal views of small-animal PET images are shown of mice imaged 6 days after tracer injection. Greater tumor intensity was observed with ^{89}Zr-AMA than ^{89}Zr-gD in the responsive OVCAR-3×2.1-, Capan-2-, and HPAC-bearing mice than in the nonresponsive AsPC-1, HPAF-II, or MSTO-211H tumors. All animals exhibited the slow uptake of bone-seeking zirconium catabolites typically seen in mice.

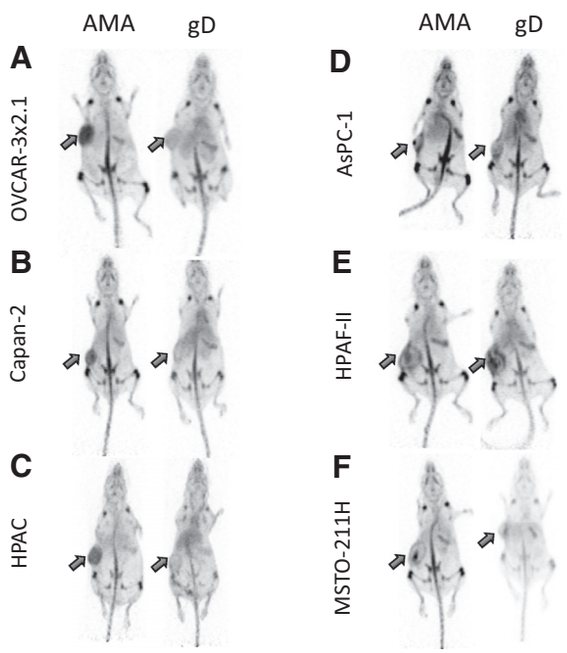

Ex vivo tumor analysis

Immunohistochemistry of xenograft tumors was used to determine whether mesothelin expression was maintained *in vivo* (Fig. 5A). OVCAR-3×2.1, AsPC-1, and HPAC showed robust staining of 3+ in malignant cells, whereas Capan-2 was 2 to 3+, HPAF-II was 2+, and MSTO-211H was 1+, in agreement with earlier results (3). Note Capan-2, HPAC, and HPAF-II show evidence of mesothelin shedding into lumens (arrows), yet shed mesothelin was undetectable (limit of detection, 0.48 ng/mL) in the blood of mice carrying HPAC or OVCAR-3×2.1 tumors. As previously reported (3), the IHC scores were higher for the xenografts than the corresponding cell pellets (data not shown), whose scores paralleled the FACS in Fig. 1. This was further confirmed by immunoprecipitation of mesothelin from xenografts and cell lines with AMA (Fig. 5B).

Figure 4.

Maximum intensity projections of PET scans from mouse coronal views of ^{89}Zr-AMA images and control (^{89}Zr-gD) antibodies in ovarian cancer OVCAR-3×2.1 (**A**); pancreatic cancers Capan-2 (**B**), HPAC (**C**), AsPC-1 (**D**), and HPAF-II (**E**); and mesothelioma MSTO-211H (**F**). Tumors are growing on the flank and indicated by arrows. The highest intensity voxel was 10 %ID/g.

Published OnlineFirst October 19, 2016; DOI: 10.1158/1535-7163.MCT-16-0449

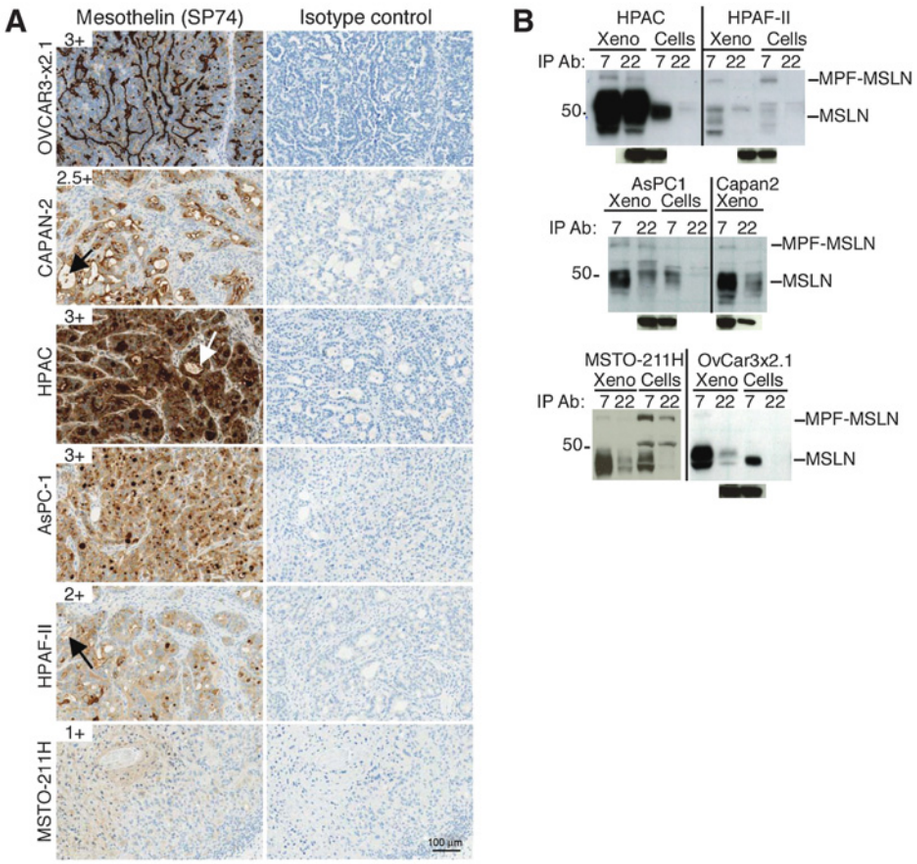

Figure 5.

A, *Ex vivo* IHC staining of representative untreated xenograft tumors with anti-mesothelin (SP74, left) or isotype control (DA1E, right). Note Capan-2, HPAC, and HPAF-II show evidence of mesothelin shedding into lumens (arrows). **B,** Mesothelin is upregulated *in vivo*. Equal amounts of xenograft (xeno) or cell line (cells) lysates were immunoprecipitated with AMA (h7D9.v3, 7) or a different lower affinity humanized anti-mesothelin antibody (h22A10.v83, 22) and Western blotted with mouse monoclonal anti-mesothelin antibody 2E5 (or 19C3 for MSTO-211H). GAPDH was used as a loading control on input lysates in a parallel blot (bottom).

An overview of the combined results is presented in Supplementary Table S2 and a correlation plot of tumor growth inhibition versus specific uptake (AMA:gD ratio) revealed a reasonable correlation ($r^2 = 0.823$; Supplementary Fig. S2).

Dose dependence of AMA pharmacokinetics and tumor growth inhibition in Capan-2 and AsPC-1 tumor–bearing mice

Because Capan-2 and AsPC-1 pancreatic models showed similar IHC expression in tumors, yet only Capan-2 responded specifically to AMA-MMAE, we confirmed the efficacy study with more mice and 2 different doses (3 and 10 mg/kg). Again, Capan-2 tumors showed dose-dependent efficacy whereas AsPC-1 did not (Fig. 6A and B). HPAC tumors were previously confirmed to respond with an IC_{50} of 3.4 mg/kg, in between that of OVCAR-3×2.1 (2.7 mg/kg) and MSTO-211H (9.3 mg/kg; ref. 3).

Pharmacokinetics (Fig. 6C) of the ADC indicated similar levels of exposure in Capan-2 and AsPC-1 and thus did not explain the differential efficacy, suggesting differential uptake might be the explanation.

To determine whether this was the case, we incubated the cell lines overnight with AMA and indeed detected internalization in OVCAR-3×2.1 and to a lesser extent Capan-2, but very little at all in HPAC or AsPC-1 (HPAF-II cells were too dim to evaluate, so MSTO-211H cells were not tested). A subset of internalized AMA colocalized with lysosomal-associated membrane protein 1 (LAMP1), indicating delivery to late endosomes and lysosomes (Fig. 6D), the target organelles for cleavage of protease-sensitive linkers such as the valine-citrulline in our ADC. Anti-gD internalization was not detectable in any cell line (bottom panel and data not shown).

Discussion

We show in this study that the tumor growth inhibition of a mesothelin targeting ADC, AMA-MMAE, correlated with ^{89}Zr-AMA immunoPET. In 6 different human xenograft models, specific tumor tracer uptake of ^{89}Zr-AMA correlated with specific efficacy of AMA-MMAE. This suggests that molecular imaging of tumor antibody uptake might have value in early drug development by identifying patients (or lesions) likely to benefit from ADC treatment.

ADCs are a promising new approach for anticancer treatment (12). However, without imaging to confirm antibody uptake in the tumor, disappointing response rates might be attributed to poor tissue penetration, absence of—or failure to bind—the target, lack of internalization, or drug resistance (12). ImmunoPET provides information about antibody tissue exposure and penetration, cell surface antigen availability, receptor internalization and recycling, and label residualization processes. It is, however, possible that the relationship between immunoPET signal and conventional expression metrics will differ from one target antigen to another and perhaps from time to time (21). Despite this caveat, the relative

Published OnlineFirst October 19, 2016; DOI: 10.1158/1535-7163.MCT-16-0449

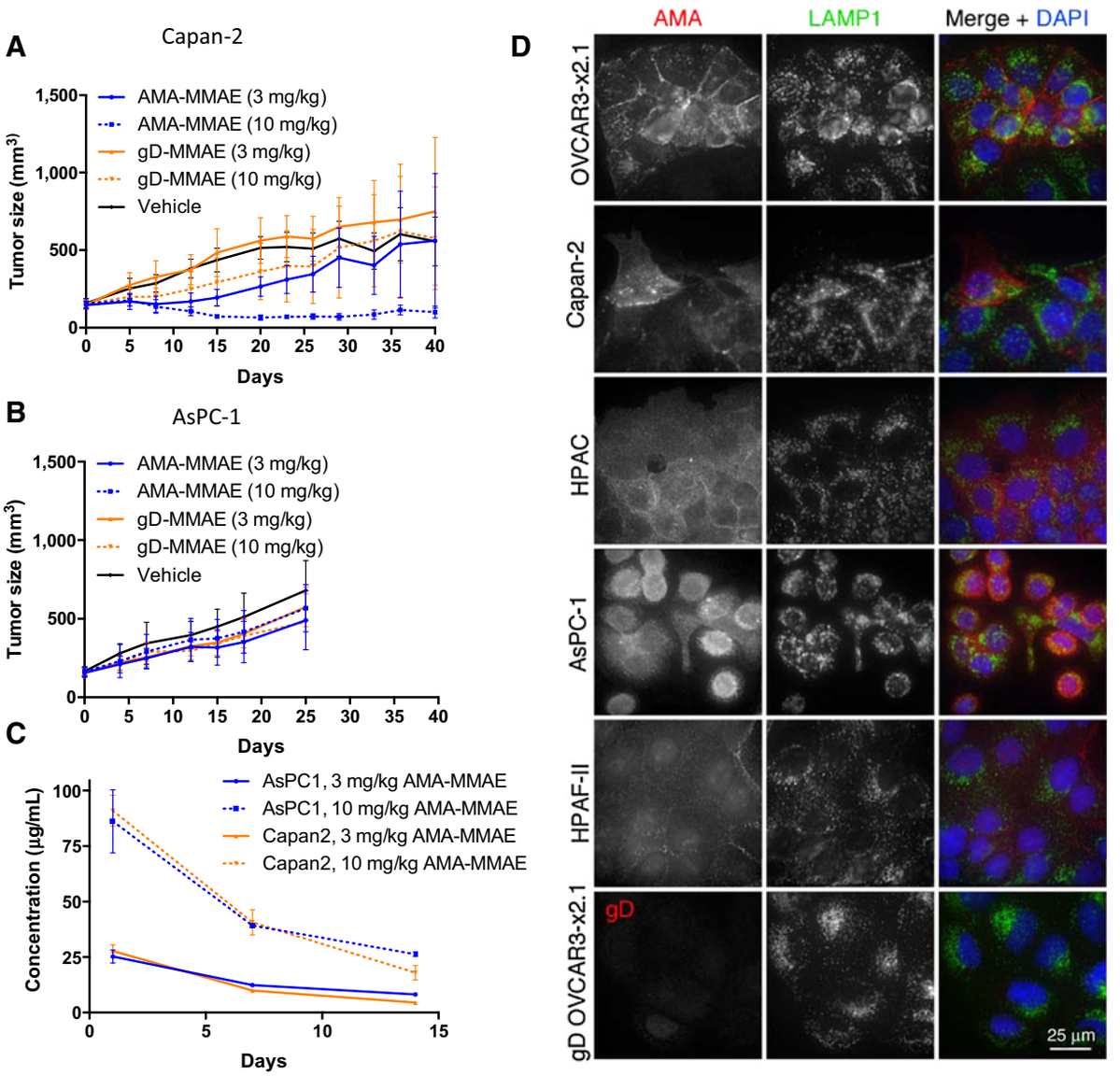

Figure 6.

Tumor growth inhibition studies in Capan-2 (**A**) and AsPC-1 (**B**) xenografts after a single dose of 3 mg/kg (solid lines) or 10 mg/kg (dashed lines) AMA-MMAE (blue) or gD-MMAE (orange) versus vehicle control (black; $n = 9$ per group) confirms differential efficacy. **C,** Serum levels of AMA in mice bearing Capan-2 (orange) or AsPC-1 (blue) tumors 0, 7, and 14 days after a single injection of 3 mg/kg (solid lines) or 10 mg/kg (dashed lines) AMA-MMAE. **D,** Deconvolution microscopy of AMA internalization in cell lines. Cells were incubated with 1 µg/mL AMA or anti-gD (bottom row) for 19 hours (in the presence of lysosomal protease inhibitors) and processed for immunofluorescence. AMA (red, left) and LAMP1 (middle, green) are overlaid with nuclear stain DAPI (4′,6-diamidino-2-phenylindole; blue, right). Scale bar is 25 µm.

immunoPET signals correctly predicted tumor growth inhibition in this study.

In OVCAR-3×2.1, Capan-2, and HPAC tumors, the ADC was efficacious, despite the relatively low levels of target-specific tumor uptake seen by imaging (only 2-fold over control), illustrating the potential of potent cytotoxic drugs when delivered as ADCs and the importance of target-mediated uptake. Mesothelin-dependent antibody uptake was relatively lower than other tumor antigens studied (i.e., HER2, EGFR; refs. 22, 23), a reflection of the relatively slow mesothelin internalization observed *in vitro*. We note that rapid internalization is no guarantee of efficacy either, illustrated in HER3 studies where xenografts with highest ^{89}Zr-RG7116 antibody uptake were not responsive to the RG7116 antibody (24, 25). Unraveling the mechanistic link between specific uptake with the imaging agent (^{89}Zr-AMA) and efficacy with the ADC (AMA-MMAE) could possibly lead to additional tissue-based predictive biomarkers to pair alongside the imaging tool. Absolute tumor uptake of ^{89}Zr-AMA is not necessarily predictive for ADC efficacy as many other factors are important to the outcome, such as cellular

sensitivity to the drug, operation of drug efflux pumps or other resistance mechanisms, variations in vascular density and permeability, as well as the nature of the extracellular matrix and the presence of noninternalizing soluble or shed mesothelin, which was observed in 3 of the models tested here (25, 26). Establishing the presence (or absence) of an antigen using molecular imaging is of importance, although it does not preclude resistance in clinical practice. When there is no cellular uptake of ^{89}Zr-AMA, minimal efficacy of AMA-MMAE can be expected; however, the converse is not necessarily true.

Our results additionally show that for predicting target-mediated ADC efficacy, distinguishing between target-specific (^{89}Zr-AMA) and nonspecific (^{89}Zr-gD) uptake is also of importance (particularly for the least ADC-responsive MSTO-211H, where the total uptake ranked second). Real (but antigen-independent) antitumor effects could be mediated through the catabolic processing of ADCs by any of the various cell types present in the tumor, through pinocytosis or processing after binding to Fcγ receptors on macrophages and monocytes (present in these mouse models), for example. If these effects were a significant contributor to ADC efficacy, this would likely weaken the association between ADC treatment effects and predictive biomarkers based on target expression. Although not trivial, this effect could potentially be controlled for in the clinic by imaging with radiolabeled pharmaceutical-grade γ-globulin as a nonspecific control reagent.

While specific tumor uptake of ^{89}Zr-AMA predicted ADC efficacy in the tumor models included in this study, our cell lines were prescreened for MMAE sensitivity, so it is to be expected that certain patient tumors might be resistant to the delivered cytotoxic drug. In this sense, immunoPET is at least noninferior to IHC because expression is necessary, but not sufficient, for efficacy. With immunoPET data, there is powerful evidence of active tumor delivery of the antibody *in situ*, which provides a rationale for considering the use of the same antibody armed with alternative cytotoxic drugs or entirely different cell death effector moieties that benefit from internalization such as radioisotopes (12).

In this study, both Capan-2 and AsPC-1 tumors stained 2 to 3+ for mesothelin expression, but tumor growth inhibition of AMA-MMAE was only achieved in the slightly lower expressing Capan-2, correlating with specific tumor uptake of ^{89}Zr-AMA. The lack of antibody uptake in AsPC-1 tumors could not be explained by reduced pharmacokinetic exposure, because the AMA showed similar clearance profiles in both models. More likely, the lower internalization rate of mesothelin in AsPC-1 cells leads to decreased ^{89}Zr tumor uptake and lower ADC efficacy (27), although the reasons for the observed differential uptake between cell lines are unclear. While shed mesothelin in the tumor microenvironment could theoretically compete with cell surface mesothelin for AMA binding *in vivo*, this did not correlate with efficacy: shed mesothelin (as detected in luminal structures by IHC) appeared highest in the responsive Capan-2 model (and nonresponsive HPAF-II, followed by HPAC) but was not observed in AsPC-1, MSTO-211H, or the most responsive OVCAR-3×2.1 (26).

There are some important caveats to be noted with murine immunoPET studies, including those presented here. First, ^{89}Zr signal accumulates in actively remodeling bone such as the knees, shoulders, and jaws, although this may be attributed to rapid metabolism of ^{89}Zr by less selective mouse liver enzymes (28). In humans, ^{89}Zr-trastuzumab and other antibodies showed very little nonspecific uptake in bone, so the suitability of ^{89}Zr-chelates for clinical imaging remains promising (29). Another potential drawback is the absence of the full human tumor immune infiltrate, with its important influence on the antitumor response in the clinic. Indeed mesothelin itself is immunogenic, producing humoral responses to tumors as well as being a successful antigen for vaccination (30, 31). A final concern is the general difference in tumor composition between homogeneous xenografts and a heterogeneous human tumor, which is particularly relevant in pancreatic cancers because of their desmoplastic tendency, with very dense stroma that can adversely affect ADC delivery. Nonetheless, the concept of using immunoPET to quantify tumor delivery in both species remains valid, and for ADCs in particular, the mechanism of action is believed to strongly depend on robust uptake in the tumor tissue.

In conclusion, quantitative data from immunoPET measuring relative antibody uptake patterns of AMA correlates with tumor growth inhibition by AMA-MMAE ADC in preclinical models. The capacity of immunoPET to demonstrate ADC delivery, binding, and internalization may thus help confirm the necessary prerequisites for efficacy with particular antibody–target combinations. Encouraged by these preclinical findings, this ^{89}Zr-AMA immunoPET has been translated to the clinic and antibody uptake has been detected in primary and metastatic pancreatic cancer and ovarian cancer tumor lesions (13). We hope that it will help predict the right patients for anti-MSLN therapies.

Disclosure of Potential Conflicts of Interest

No potential conflicts of interest were disclosed.

Authors' Contributions

Conception and design: A.G.T.T. van Scheltinga, A. Ogasawara, J. Malik, S.J. Scales, S.-P. Williams

Development of methodology: A. Ogasawara, J. Malik, S.-P. Williams

Acquisition of data (provided animals, acquired and managed patients, provided facilities, etc.): A. Ogasawara, G. Pacheco, A. Vanderbilt, J. Tinianow, N. Gupta, J. Malik, S.J. Scales, S.-P. Williams

Analysis and interpretation of data (e.g., statistical analysis, biostatistics, computational analysis): A.G.T.T. van Scheltinga, A. Ogasawara, G. Pacheco, A. Vanderbilt, J. Tinianow, D. Li, R. Firestein, J. Malik, S.J. Scales, S.-P. Williams

Writing, review, and/or revision of the manuscript: A.G.T.T. van Scheltinga, A. Ogasawara, G. Pacheco, D. Li, J. Malik, S.J. Scales, S.-P. Williams

Administrative, technical, or material support (i.e., reporting or organizing data, constructing databases): A. Ogasawara, D. Li, S.-P. Williams

Study supervision: S.-P. Williams

Other (*in vivo* principal investigator): G. Pacheco

Acknowledgments

The authors would like to thank Susan Spencer, Paul Polakis, Kathy Kozak, Aimee Fourie, Elizabeth Luis, Herman Gill, Jay Tibbitts, Linda Rangell, and Sarajane Ross for their advice and help with this work.

The costs of publication of this article were defrayed in part by the payment of page charges. This article must therefore be hereby marked *advertisement* in accordance with 18 U.S.C. Section 1734 solely to indicate this fact.

Received July 11, 2016; revised September 27, 2016; accepted September 29, 2016; published OnlineFirst October 19, 2016.

Published OnlineFirst October 19, 2016; DOI: 10.1158/1535-7163.MCT-16-0449

References

1. Argani P, Iacobuzio-Donahue C, Ryu B, Rosty C, Goggins M, Wilentz RE, et al. Mesothelin is overexpressed in the vast majority of ductal adenocarcinomas of the pancreas: identification of a new pancreatic cancer marker by serial analysis of gene expression (SAGE). Clin Cancer Res 2001;7:3862–8.
2. Frierson HF Jr, Moskaluk CA, Powell SM, Zhang H, Cerilli LA, Stoler MH, et al. Large-scale molecular and tissue microarray analysis of mesothelin expression in common human carcinomas. Hum Pathol 2003;34:605–9.
3. Scales SJ, Gupta N, Pacheco G, Firestein R, French DM, Koeppen H, et al. An antimesothelin-monomethyl auristatin e conjugate with potent antitumor activity in ovarian, pancreatic, and mesothelioma models. Mol Cancer Ther 2014;13:2630–40.
4. Katz J, Janik JE, Younes A. Brentuximab Vedotin (SGN-35). Clin Cancer Res 2011;17:6428–36.
5. Doronina SO, Toki BE, Torgov MY, Mendelsohn BA, Cerveny CG, Chace DF, et al. Development of potent monoclonal antibody auristatin conjugates for cancer therapy. Nat Biotechnol 2003;21:778–84.
6. Verma S, Miles D, Gianni L, Krop IE, Welslau M, Baselga J, et al. Trastuzumab emtansine for HER2-positive advanced breast cancer. N Engl J Med 2012;367:1783–91.
7. Hassan R, Miller AC, Sharon E, Thomas A, Reynolds JC, Ling A, et al. Major cancer regressions in mesothelioma after treatment with an anti-mesothelin immunotoxin and immune suppression. Sci Transl Med 2013;5:208ra147.
8. Hassan R, Sharon E, Thomas A, Zhang J, Ling A, Miettinen M, et al. Phase 1 study of the antimesothelin immunotoxin SS1P in combination with pemetrexed and cisplatin for front-line therapy of pleural mesothelioma and correlation of tumor response with serum mesothelin, megakaryocyte potentiating factor, and cancer antigen 125. Cancer 2014;120:3311–9.
9. Golfier S, Kopitz C, Kahnert A, Heisler I, Schatz CA, Stelte-Ludwig B, et al. Anetumab ravtansine: a novel mesothelin-targeting antibody-drug conjugate cures tumors with heterogeneous target expression favored by bystander effect. Mol Cancer Ther 2014;13:1537–48.
10. Polakis P. Antibody drug conjugates for cancer therapy. Pharmacol Rev 2016;68:3–19.
11. Weekes CD, Lamberts LE, Borad MJ, Voortman J, McWilliams RR, Diamond JR, et al. Phase I study of DMOT4039A, an antibody-drug conjugate targeting mesothelin, in patients with unresectable pancreatic or platinum-resistant ovarian cancer. Mol Can Ther 2016;15:439–47.
12. Sievers EL, Senter PD. Antibody-drug conjugates in cancer therapy. Annu Rev Med 2013;64:15–29.
13. Lamberts LE, Menke-van der Houven van Oordt CW, Ter Weele EJ, Bensch F, Smeenk MM, Voortman J, et al. ImmunoPET with anti-mesothelin antibody in patients with pancreatic and ovarian cancer before anti-mesothelin antibody-drug conjugate treatment. Clin Cancer Res 2016;22:1642–52.
14. ter Weele EJ, Terwisscha van Scheltinga AG, Kosterink JG, Pot L, Vedelaar SR, Lamberts LE, et al. Imaging the distribution of an antibody-drug conjugate constituent targeting mesothelin with ^{89}Zr and IRDye 800CW in mice bearing human pancreatic tumor xenografts. Oncotarget 2015;6:42081–90.
15. Lamberts LE, Williams SP, Terwisscha van Scheltinga AG, Lub-de Hooge MN, Schröder CP, Gietema JA, et al. Antibody positron emission tomography imaging in anticancer drug development. J Clin Oncol 2015;33:1491–504.
16. Yoshida C, Sogawa C, Tsuji AB, Sudo H, Sugyo A, Uehara T, et al. Development of positron emission tomography imaging by 64Cu-labeled Fab for detecting ERC/mesothelin in a mesothelioma mouse model. Nucl Med Commun 2010;31:380–8.
17. Kobayashi K, Sasaki T, Takenaka F, Yakushiji H, Fujii Y, Kishi Y, et al. A novel PET imaging using 64Cu-labeled monoclonal antibody against mesothelin commonly expressed on cancer cells. J Immunol Res 2015;2015:268172.
18. Lindenberg L, Thomas A, Adler S, Mena E, Kurdziel K, Maltzman J, et al. Safety and biodistribution of 111In-amatuximab in patients with mesothelin expressing cancers using single photon emission computed tomography-computed tomography (SPECT-CT) imaging. Oncotarget 2015;6:4496–504.
19. Lin K, Tibbitts J. Pharmacokinetic considerations for antibody drug conjugates. Pharm Res 2012;29:2354–66.
20. Vosjan MJ, Perk LR, Visser GW, Budde M, Jurek P, Kiefer GE, et al. Facile radiolabeling of monoclonal antibodies and other proteins with zirconium-89 or gallium-68 for PET imaging using p-isothiocyanatobenzyl-desferrioxamine. Nat Protoc 2010;5:739–43.
21. Williams SP.Tissue distribution studies of protein therapeutics using molecular probes: molecular imaging. AAPS J 2012;14:389–99.
22. Dijkers EC, Kosterink JG, Rademaker AP, Perk LR, van Dongen GA, Bart J, et al. Development and characterization of clinical-grade 89Zr-trastuzumab for HER2/neu immunoPET imaging. J Nucl Med 2009;50:974–81.
23. Aerts HJ, Dubois L, Perk L, Vermaelen P, van Dongen GA, Wouters BG, et al. Disparity between in vivo EGFR expression and 89Zr-labeled cetuximab uptake assessed with PET. J Nucl Med 2009;50:123–31.
24. Mirschberger C, Schiller CB, Schraml M, Dimoudis N, Friess T, Gerdes CA, et al. RG7116, a therapeutic antibody that binds the inactive HER3 receptor and is optimized for immune effector activation. Cancer Res 2013;73:5183–94.
25. Terwisscha van Scheltinga AG, Lub-de Hooge MN, Abiraj K, Schröder CP, Pot L, Bossenmaier B, et al. ImmunoPET and biodistribution with human epidermal growth factor receptor 3 targeting antibody 89Zr-RG7116. MAbs 2014;6:1051–8.
26. Pastan I, Zhang Y. Modulating mesothelin shedding to improve therapy. Oncotarget 2012;3:114–5.
27. Perera RM, Zoncu R, Johns TG, Pypaert M, Lee FT, Mellman I, et al. Internalization, intracellular trafficking, and biodistribution of monoclonal antibody 806: a novel anti-epidermal growth factor receptor antibody. Neoplasia 2007;9:1099–110.
28. Abou DS, Ku T, Smith-Jones PM. In vivo biodistribution and accumulation of 89Zr in mice. Nucl Med Biol 2011;38:675–81.
29. Dijkers EC, Oude Munnink TH, Kosterink JG, Brouwers AH, Jager PL, de Jong JR, et al. Biodistribution of 89Zr-trastuzumab and PET imaging of HER2-positive lesions in patients with metastatic breast cancer. Clin Pharmacol Ther 2010;87:586–92.
30. Le DT, Wang-Gillam A, Picozzi V, Greten TF, Crocenzi T, Springett G, et al. Safety and survival with GVAX pancreas prime and Listeria Monocytogenes-expressing mesothelin (CRS-207) boost vaccines for metastatic pancreatic cancer. J Clin Oncol 2015;33:1325–33.
31. Zhang Y, Choi M. Immune therapy in pancreatic cancer: now and the future? Rev Recent Clin Trials 2015;10:317–25.